Available online at www.sciencedirect.com
ScienceDirect
International Journal of Thermal Sciences 48 (2009) 133–145
International Journal of Thermal Sciences
www.elsevier.com/locate/ijts

Modelling of the operation of Polymer Exchange Membrane Fuel Cells in the presence of electrodes flooding

O. Lottin [a,*], B. Antoine [a], T. Colinart [a], S. Didierjean [a], G. Maranzana [a], C. Moyne [a], J. Ramousse [b]

[a] *LEMTA, Nancy-University, CNRS, 2, avenue de la forêt de Haye, BP 160, 54504 Vandoeuvre-lès-Nancy cedex, France*
[b] *Institut de Recherche sur l'Hydrogène, Université de Québec Trois-Rivières, 3351 boulevard des Forges, C.P. 500, G9A 5H7 Trois-Rivières (QC), Canada*

Received 28 June 2007; received in revised form 12 March 2008; accepted 15 March 2008

Available online 21 April 2008

Abstract

This paper presents a simple pseudo-2D model of Polymer Exchange Membrane Fuel Cell including mass transport limitation due to flooding. The gas channels are assumed parallel to the membrane and the changes in gas composition due to the electro-chemical reactions are taken into account. The overpotentials at anode and cathode are evaluated by a Tafel law while a simple reasoning about heat transfer shows that at the highest intensities, liquid water appears at the cathode-backing layers interface. It is assumed that the appearance of liquid defines the local value of the limiting current density. The results of this model differ from those obtained with a conventional 1D approach when there is a high difference in water inlet concentration between hydrogen and air channels. Furthermore, the pseudo-2D model proposes a credible representation of the high-intensity range of the polarization curve, and allows to determine the limiting current in the whole cell, as a function of gases hydration.

Keywords: Fuel cells; Membrane; Electrode flooding; Modelling; Polarization curve; Pseudo-bidimensional

1. Introduction

The difficulties in modelling the operation of PEMFC come as much from the complexity of coupled phenomena of mass, heat and charge transfer occurring in the Membrane Electrodes Assembly (MEA), as from the complexity of the geometry of a single cell: the bipolar plates, backing layers, electrodes and membrane are made of materials of very different size and structure. Furthermore, the geometry of the flows of hydrogen and air is tri-dimensional and the presence of liquid water must be taken into account. The bi- or tri-dimensional models that take account of fluid dynamics and molar changes along the gas channels lead to heavy and complex simulation software [1–4], especially when two-phase flows are considered [5]. However, Costamagna [6], Costamagna and Srinivasan [7] and Djilali and Lu [8] suggested that a multidimensional model is necessary for an accurate description of PEMFC operation, since the gas composition and the temperature vary along the gas channels. Recent attempts in quasi-two-dimensional modelling were accomplished. Dannenberg et al. [9] accounted for heat removal into a coolant but assumed constant temperature in the through-plane direction. Janssen [10] focused on the water management to compare the results with her experimental data, but homogeneous current density distribution was assumed. Berg et al. [11] assumed a fully isothermal cell, but neglected the transport of species in the Gas Diffusion Layers (GDL) and the liquid water transport. Bautista et al. [12] proposed also a pseudo bi-dimensional description using a Gas Diffusion Electrode for modelling the active layer. However, no assumption was made about mass transport limitation due to flooding. Recently, Freundberger et al. [13] proposed a non-isothermal description of the cell and considered the liquid water transport in the GDL in terms of gradient of the chemical potential in the liquid phase. The reaction limitation was taken into account in terms of limiting current.

Water management is one of the main difficulties with the operation of fuel cell. First of all because the membrane plays a key role in fuel cell performances while its ionic conductiv-

* Corresponding author.
E-mail address: Olivier.Lottin@ensem.inpl-nancy.fr (O. Lottin).

1290-0729/$ – see front matter
doi:10.1016/j.ijthermalsci.2008.03.013

Nomenclature

a	activity coefficient	
D	diffusion coefficient	$m^2\,s^{-1}$
e_l	liquid layer thickness (in the GDL)	m
e_{dry}	dry layer thickness (in the GDL)	m
F	Faraday constant	96485 $C\,mol^{-1}$
g	Gibbs free energy	$J\,mol^{-1}$
$K_{dry\ layer}$	mass transfer resistance	$mol\,s^{-1}$
I	intensity	A
i	current density	$A\,m^{-2}$
i_0	exchange current density	$A\,m^{-2}$
i_l	limiting current density	$A\,m^{-2}$
l_a	anode GDL total thickness	m
l_c	cathode GDL total thickness	m
l_m	membrane thickness	m
M	molecular mass	$g\,mol^{-1}$
$\dot{N}$	molar flux	$mol\,s^{-1}$
p	pressure or partial pressure	Pa
$\dot{Q}$	heat flux	W
S	cell surface	m^2
T	temperature	K
$\dot{W}$	electric power	W
x	coordinate perpendicularly to the membrane	m
y	mole fraction	$mol\,mol^{-1}$
z	coordinate parallel to the membrane	m
ε	porosity	
η	polarization (activation, concentration or ohmic)	V
ρ	resistivity	ohm m

Subscripts

a	anode
act	activation
c	cathode
cr	critical
con	concentration
e	electrolyte
Ohm	ohmic
i	chemical species (H_2, H_2O or O_2)
I	feeding channels inlet
k	number of slice

Superscripts

0	Standard conditions (298 K and 10^5 Pa)

ity is highly dependent on its water content. However, it is well known that an excess of water lead to the appearance of liquid droplets in the gas channels and/or in the GDL and on the electrodes [14]: broadly speaking, the effect of liquid water is to restrict the access of reactant gases to the catalyst, thus lowering the cell voltage. Accounting for flooding and its effects on performances is probably one of the trickiest issues in fuel cell modelling, because it implies considering phase changes and two-phase flows in very different media (gas channels, gas diffusion layers and electrodes).

This paper presents a model of PEMFC single cell, intended not to be very demanding in terms of computation time, but to take account of most of the physical phenomena, including flooding, and of part of the effects of fuel and air distribution by the bipolar plates. The computing time is of the order of tenths of seconds for a working point with a regular personal computer (a few minutes for a full polarization curve). This model is close to those of Berg et al. [11], Bautista et al. [12] and Freundberger et al. [13] in the sense that it can be considered as *quasi-* or *pseudo*-two-dimensional. In this way, only the most relevant phenomena occurring in each of the main directions are retained, at the profit of the computation time. However, new hypotheses are introduced to account for the flooding of the electrodes. As shown below, the model allows to determine the fuel cell limiting current density as a function of the gas composition and stoichiometry only.

The cell geometry is planar and the flows in the feeding channels are considered as uniform (in velocity and concentrations) in one direction parallel to the electrolyte (z in Fig. 1, not represented). The velocity and the concentrations can vary in the second direction parallel to the electrolyte (x in Fig. 1). Mass transport in the electrodes and electrolyte are assumed to occur only in the direction perpendicular to the membrane (y in Fig. 1). This model is called pseudo-2D since gases concentration and flow rate variations are described in one direction in the gas channels and in another (perpendicular) direction in the electrodes and electrolyte. The thickness of the electrode active layers is considered negligible (surface electrodes) by comparison with the thickness of the porous backing layers and electrolyte. Each horizontal slice k in Fig. 1 is considered as an independent 1D fuel cell fed with gases which molar composition results from mass balance at slice $k-1$. Current densities J_k at each slice are assumed to depend on local gases composition and on fuel cell pressure and potential.

Following Ramousse et al. [15,16], who showed that PEMFC gas diffusion electrodes exhibit Tafel behavior in steady state, the overpotentials at anode and cathode are evaluated by Tafel law. The molar flux of species through the anode and cathode porous backing layers is calculated analytically by mean of the Stefan–Maxwell equations. The temperature is assumed uniform in the whole cell and consequently, a strong hypothesis is done about the location where water condensates, supposed to be the cathode-backing layer interface. The appearance of liquid defines the local value of the limiting current density.

The hypotheses governing the modelling of mass and charge transfer in the direction perpendicular to the membrane are depicted in the following section. The pseudo-2D approach is described briefly in the third section and some results are presented in the fourth section. A discussion about the local heterogeneities put forward by the model is opened in the last section before conclusion, on the basis of published experimental results.

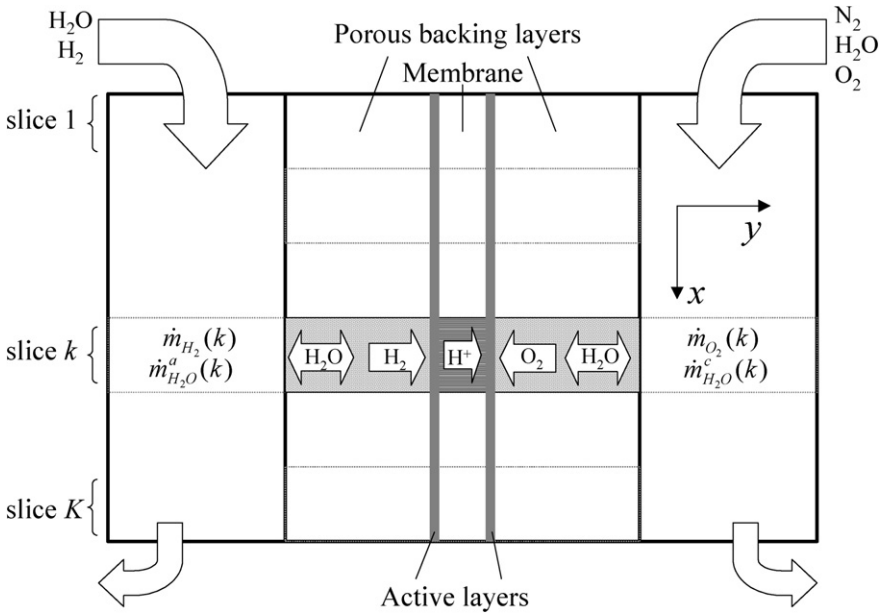

Fig. 1. Simplified cell representation for modelling. The thickness of the active layers (bold lines) is neglected.

2. Mass and charge transfer in a slice

At the anode, H_2 is oxidized (1), liberating electrons and producing protons. The electrons flow to the cathode *via* an external circuit and combine with the protons and the oxidant (oxygen) to produce water (2). Proton transfer from the anode to the cathode through the polymer membrane closes the electrical circuit. From an energetic point of view, the overall reaction (3) differs from hydrogen combustion because part of the Gibbs free energy is converted into electric energy.

$$\text{Anode} \qquad H_2 \rightarrow 2H^+ + 2e^- \tag{1}$$

$$\text{Cathode} \qquad \frac{1}{2}O_2 + 2H^+ + 2e^- \rightarrow H_2O_v \tag{2}$$

$$\text{Overall reaction} \qquad H_2 + \frac{1}{2}O_2 \rightarrow H_2O_v \tag{3}$$

2.1. Mass transfer in the absence of liquid water

The source terms are the molar rate of hydrogen and oxygen consumed (negative sign) at the anodic and cathodic active layers, respectively, and the molar rate of water produced in vapor phase at the cathodic active layer (positive sign). They are given by the following expressions:

$$\dot{N}_{H_2} = -\frac{i_{cell}}{2F}; \qquad \dot{N}_{O_2} = -\frac{i_{cell}}{4F}; \qquad \dot{N}_{H_2O} = \frac{i_{cell}}{2F} \tag{4}$$

The thickness of the active layers is neglected: they are considered as interfaces between the membrane and the backing layers. The membrane being impervious to gases, hydrogen and oxygen only flows from the feeding channels to the active layers. Only water can pass through the membrane, in a direction depending on current density and on gas hydration [17,18] (5). Fluxes are considered positive in the y-direction (Fig. 1).

$$\dot{N}^c_{H_2O} = \frac{i_{cell}}{2F} + \dot{N}^m_{H_2O} \quad \text{and} \quad \dot{N}^a_{H_2O} = \dot{N}^m_{H_2O} \tag{5}$$

Where superscripts *a, c* and *m* refer to **a**node and **c**athode sides and **m**embrane.

Stefan–Maxwell equations are used in most of the models of the literature to describe gas diffusion in the backing layers (6) [19,20]:

$$\frac{dy_i}{dx} = \frac{RT}{P}\sum_i \frac{y_i\dot{N}_j - y_j\dot{N}_i}{D^{\text{eff}}_{i,j}} \tag{6}$$

$$\sum_i y_i = 1 \quad \text{at both anode and cathode sides}$$

$$i, j = H_2, H_2O_{gas} \quad \text{at the anode side} \quad \text{and}$$

$$i, j = O_2, N_2, H_2O_{gas} \quad \text{at the cathode side} \tag{7}$$

The backing layers being porous, it is necessary to use effective diffusion coefficients (8) [21]:

$$D^{\text{eff}}_{i,j} = \varepsilon^{3/2} D^{\text{eff}}_{i,j} \tag{8}$$

Considering the molar flux densities of water in the anodic and cathodic backing layers (5) as parameters, and using the concentration of gases in the feeding channels as boundary conditions, Eq. (6) leads to the following analytic expressions for concentration distributions (9)–(17).

- In the anodic backing layer $x = 0$ at the GDL-channel interface and $x = l_a$ at the anode-GDL interface. The boundary condition $y^0_{H_2}$ is the molar concentration in the hydrogen channel ($x = 0$). The analytical expressions are reported in Table 1. For convenience, the coefficients

$$k_a = \frac{\dot{N}_{H_2} + \dot{N}^m_{H_2O}}{cD^{\text{eff}}_{H_2,H_2O}} \quad \text{and} \quad c = \frac{P}{RT}$$

  are introduced in the equations $y^a_{H_2O} = 1 - y_{H_2O}(x)$.
- In the cathodic backing layer $x = 0$ at the cathode-GDL interface and $x = l_c$ at the GDL-channel interface. The

Table 1
Solution of Stefan–Maxwell equations in the anodic GDL

$k_a = 0$	$y_{H_2} = y^0_{H_2} - \dfrac{\dot{N}_{H_2}}{cD^{eff}_{H_2,H_2O}}$	(9)
$k_a \neq 0$	$y_{H_2} = \dfrac{\dot{N}_{H_2}}{\dot{N}_{H_2}+\dot{N}^m_{H_2O}} + \left(y^0_{H_2} - \dfrac{\dot{N}_{H_2}}{\dot{N}_{H_2}+\dot{N}^m_{H_2O}}\right)e^{k_a x}$	(10)

boundary conditions $y^0_{O_2}$ and $y^0_{N_2}$ are the molar concentrations in the gas channels ($x = l_c$) and $y^c_{H_2O} = 1 - y_{O_2}(x) - y_{N_2}(x)$. The equations are reported in Table 2. The coefficients

$$k_n = \frac{\dot{N}^m_{H_2O}}{cD^{eff}_{N_2,H_2O}} + \frac{\dot{N}_{O_2}}{cD^{eff}_{N_2,O_2}}, \qquad k_c = \frac{\dot{N}^m_{H_2O} + \dot{N}_{O_2}}{cD^{eff}_{O_2,H_2O}}$$

$$k_D = \frac{1}{cD^{eff}_{O_2,H_2O}} - \frac{1}{cD^{eff}_{O_2,N_2}} \quad \text{and} \quad c = \frac{P}{RT}$$

are introduced for convenience.

In the membrane, the phenomenological model proposed by Springer et al. [10] is retained, in which the water content λ is defined as the number of water moles per mole of sulfonic acid (18):

$$\lambda = \frac{EW}{\rho_{dry}} c_{H_2O} \tag{18}$$

where EW (equivalent weight) represents the dry membrane weight per mole of sulfonate group (kg/mol); ρ_{dry} is the density of dry polymer (kg/m^3).

According to Okada et al. [17,18], the water electro-osmotic flux through the membrane, always directed from anode to cathode, is a linear function of the proton flux imposed by the current density:

$$\dot{N}^{osmotic}_{H_2O} = \tau \frac{i_{cell}}{F} \quad \text{and} \quad \tau = \lambda\tau_0 \tag{19}$$

where τ stands for the water molecules number dragged by a proton. τ_0 is the electro-osmotic drag coefficient (Table 1).

The water diffusion flux $\dot{N}^{diff}_{H_2O}$ through the membrane depends linearly on the water concentration gradient. The sum of diffusion and electro-osmotic fluxes yields a first order differential equation in λ:

$$\dot{N}^m_{H_2O} = \dot{N}^{osmotic}_{H_2O} + \dot{N}^{diff}_{H_2O} = \lambda\tau_0 \frac{i_{cell}}{F} - D_m \frac{\rho_{dry}}{EW}\frac{d\lambda}{dx} \tag{20}$$

And the solution of Eq. (20) is:

$$\frac{\lambda(x) - \lambda_a}{\lambda_c - \lambda_a} = \frac{1 - e^{k_m x}}{1 - e^{k_m l_m}} \tag{21}$$

$$\dot{N}^m_{H_2O} = \tau_0 \frac{F}{i_{cell}}\left[\lambda_a + \frac{\lambda_c - \lambda_a}{1 - e^{k_m l_m}}\right] \quad \text{with } k_m = \frac{EW \cdot \tau_0 \cdot i_{cell}}{\rho_{dry} D_m F} \tag{22}$$

where λ_c and λ_a stand for membrane water content at the electrolyte/cathode and membrane/anode interfaces, respectively.

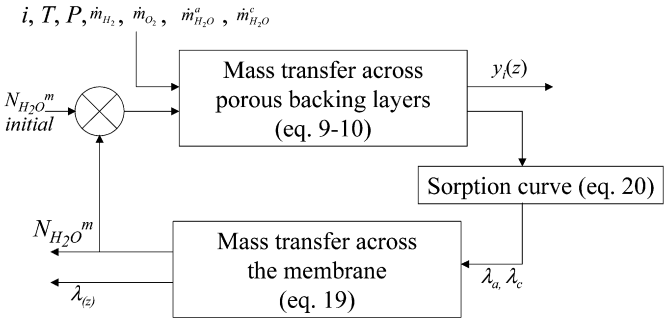

Fig. 2. Solving algorithm.

Thermodynamic equilibrium between vapor in the backing layers and liquid water in the membrane is assumed and the sorption curve of Hinatsu et al. [23] is used to determine λ_a and λ_c as functions of vapor partial pressure:

$$\lambda = 0.3 + 10.8\left(\frac{p_{H_2O}}{P_{sat}}\right) - 16\left(\frac{p_{H_2O}}{P_{sat}}\right)^2 + 14.1\left(\frac{p_{H_2O}}{P_{sat}}\right)^3 \tag{23}$$

The solving algorithm (Fig. 2) determines first the water concentrations at the active layers/membrane interfaces that satisfy Eqs. (9)–(17) and then the water flux through de membrane using Eqs. (20)–(22). The initial value of the water flux is arbitrarily chosen and the loop is repeated until convergence.

2.2. Mass transfer considering flooding

Since the cell is assumed isothermal, water must condense first where it is produced (where partial pressure of vapor is the highest), that is to say at cathode-membrane interface. A simple assumption allows the calculation of the thickness of liquid layer overlaying the cathode: it is supposed that the liquid layer grows until the remaining dry side of the porous backing layer is thin enough to allow the evacuation of water by gas diffusion only. The main interest of this description, beyond its simplicity, is not to require any supplementary (unknown) parameter. It relies on backing layer hydrophobicity (the presence of a liquid flux being therefore questionable) and remains valid whatever the current density crossing the cell: providing the dry layer is thin enough, it is always possible to evacuate water by gas diffusion only (Fig. 3).

The curve of Fig. 3 reflects the decrease in the mass transfer resistance of the dry layer with the growing thickness of the liquid layer (with the reduction of the dry layer thickness). For clarity, it is possible to rewrite the expression of the water flux through the backing layer as:

$$\dot{N}^c_{H_2O} = \frac{i_{cell}}{2F} + \dot{N}^m_{H_2O} = K_{dry\ layer}(e_{dry}) \cdot \left[y_{H_2O}(\text{liquid–gas interface}) - y_{H_2O}(\text{cathode})\right] \tag{24}$$

Where $K_{dry\ layer}$ denotes the mass transfer resistance of the dry layer, assuming that it is a growing function of its thickness e_{dry}. There is no simple expression for $K_{dry\ layer}$. In Fig. 3, the GDL remains entirely dry for i_{cell} ranging from 0 A/m^2

Table 2
Solution of Stefan–Maxwell equations in the cathodic GDL

$k_n = 0$	$k_c = 0$	$y_{N_2} = y^0_{N_2}$	(11)
		$y_{O_2} = y^0_{O_2} + \left[y^0_{N_2} \dot{N}_{O_2} k_D - \dfrac{\dot{N}_{O_2}}{c D^{\text{eff}}_{O_2,H_2O}} \right](v - l_c)$	(12)
	$k_c \neq 0$	$y_{N_2} = y^0_{N_2}$	(11)
		$y_{O_2} = \left[y^0_{O_2} + \left(y^0_{N_2} \dot{N}_{O_2} k_D - \dfrac{\dot{N}_{O_2}}{c D^{\text{eff}}_{O_2,H_2O}} \right) \dfrac{l}{k_c} \right] e^{k_n (x - l_c)} - \left(y^0_{N_2} \dot{N}_{O_2} k_D - \dfrac{\dot{N}_{O_2}}{c D^{\text{eff}}_{O_2,H_2O}} \right)$	(13)
$k_n \neq 0$	$k_c = 0$	$y_{N_2} = y^0_{N_2} e^{k_n (x - l_c)}$	(14)
		$y_{O_2} = y^0_{O_2} - \dfrac{\dot{N}_{O_2}}{c D^{\text{eff}}_{O_2,H_2O}} (x - l_c) + \dfrac{y^0_{N_2} \dot{N}_{O_2} k_D}{k_n} (e^{k_n (x - l_c)} - 1)$	(15)
	$k_c \neq 0$		
	$k_n - k_c = 0$	$y_{N_2} = y^0_{N_2} e^{k_n (x - l_c)}$	(14)
		$y_{O_2} = \left(y^0_{O_2} - \dfrac{\dot{N}_{O_2}}{c D^{\text{eff}}_{O_2,H_2O}} \dfrac{l}{k_c} \right) e^{k_c (x - l_c)} + y^0_{N_2} \dot{N}_{O_2} k_D (x_c - l_c) \dfrac{e^{k_c x}}{e^{k_n l_c}} + \dfrac{\dot{N}_{O_2}}{c D^{\text{eff}}_{O_2,H_2O}} \dfrac{l}{k_c}$	(16)
	$k_n - k_c \neq 0$	$y_{N_2} = y^0_{N_2} e^{k_n (x - l_c)}$	(14)
		$y_{O_2} = \left(y^0_{O_2} - \dfrac{\dot{N}_{O_2}}{c D^{\text{eff}}_{O_2,H_2O}} \dfrac{l}{k_c} - \dfrac{y^0_{N_2} \dot{N}_{O_2}}{k_n - k_c} k_D \right) e^{k_c (x - l_c)} + \dfrac{y^0_{N_2} \dot{N}_{O_2}}{k_n - k_c} k_D e^{k_n (x - l_c)} + \dfrac{\dot{N}_{O_2}}{c D^{\text{eff}}_{O_2,H_2O}} \dfrac{l}{k_c}$	(17)

Table 3
Numerical value of the parameters

Parameter	Numerical value	Refs
$L_a = L_c$	$230 \cdot 10^{-6}$ m	This work
L_m	$125 \cdot 10^{-6}$ m	This work
ϵ_{back}	0.8	[20]
EW	1.1 kg mole^{-1}	[17]
ρ_{dry}	2020 kg m^{-3}	[17]
τ_0	2.5/22	[17]
D_m	$3 \cdot 10^{-10}$ m^2 s^{-1}	[17]
D_{H_2,H_2O}	$1.63 \cdot 10^{-4}$ m^2 s^{-1}	[24]
D_{O_2,H_2O}	$3.20 \cdot 10^{-5}$ m^2 s^{-1}	[24]
D_{O_2,N_2}	$2.41 \cdot 10^{-5}$ m^2 s^{-1}	[24]
D_{N_2,H_2O}	$3.35 \cdot 10^{-5}$ m^2 s^{-1}	[24]
$H = \dfrac{C_{O_2,g}}{C_{O_2,l}}$	25	[25]
D_{O_2,H_2O_l} (diffusion in the polymer)	$5 \cdot 10^{-11}$ m^2/s	[25]
D_{O_2,H_2O_l}	$1.2 \cdot 10^{-10}$ m^2/s^{-1}	[22]
$K = \dfrac{P_{O_2}}{C_{O_2,l}}$	$2 \cdot 10^5$ atm cm^3/mol	

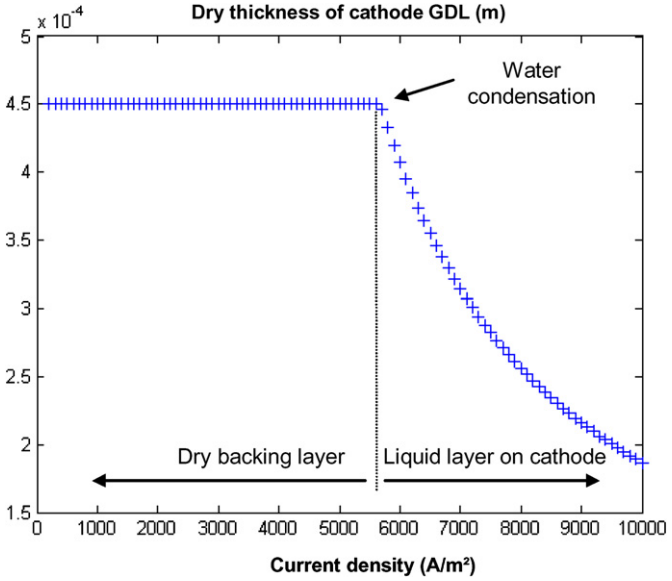

Fig. 3. Dry thickness (m) in the porous backing layer as a function of the current density. The liquid water layer overlaying the electrodes appears when the current density reaches 5700 A/m^2. (Thickness of the porous backing layer: 450 μm; thickness of the membrane: 30 μm (Nafion); dew temperature of the air: 79 °C; dew temperature of the hydrogen: 79 °C; fuel cell temperature: 80 °C.)

to 5700 A/m^2 ($e_{\text{dry}} = l_c$) and the rise in $\dot{N}^c_{H_2O}$ ($y^0_{H_2O}$ being constant) is compensated by an increase in $y^c_{H_2O}$. After $y^c_{H_2O}$ reached $y^{\text{sat}}_{H_2O}$, the rise in $\dot{N}^c_{H_2O}$ (for i_{cell} increasing above 5700 A/m^2) is compensated by the reduction of the GDL dry thickness e_{dry}.

However, oxygen diffusion through the liquid layer drastically limits its thickness: oxygen is assumed to move in liquid water by molecular diffusion; as it is very diluted, its concentration profile is linear in steady state. Therefore, the molar flux

of oxygen through the liquid layer (as a function of z) is given by:

$$\dot{N}_{O_2} = \frac{-i}{4F} = D_{O_2,H_2O_l} \frac{c_{O_2,l}(\text{cathode}) - c_{O_2,l}(\text{liquid–gas interface})}{e_l} \quad (25)$$

Where e_l is the thickness of the liquid layer. The concentration of dissolved oxygen at gas–liquid interface is given by the ratio between oxygen partial pressure p_{O_2} and Henry coefficient K_{O_2} (Table 1):

$$c_{O_2,l}(\text{liquid–gas interface}) = \frac{p_{O_2}}{K_{O_2}} \quad (26)$$

Eqs. (24) and (25) allows to derive the oxygen concentration at the cathode (26) and then deducing the concentration overvoltage due to oxygen diffusion in water.

$$c_{O_2,l}(\text{cathode}) = \frac{p_{O_2}}{K_{O_2}} - \frac{i e_l}{4F D_{O_2,H_2O_l}} \quad (27)$$

2.3. Charge transfer

The following equations allow to estimate the fuel cell potential E as a function of the current density i. E is expressed as follows:

$$E = E_{Gibbs} - R_m i - \eta_{act} \quad (28)$$

where R_m is the membrane ohmic resistance, η_{act} is the activation overvoltage and E_{Gibbs} is the cell thermodynamic potential estimated from Gibbs free energy of hydrogen combustion reaction (as a function of reagents concentration at active layers).

The ohmic resistance of the membrane R_m is derived from Neubrand's correlation [26] that yields the ionic conductivity of Nafion® as a function of membrane water content λ (18) and temperature T:

$$\sigma = (0.2856\lambda + 0.0298\lambda^2 + 0.0013\lambda^3) \exp\left[-E\left(\frac{1}{T} - \frac{1}{T_{ref}}\right)\right] \quad (29)$$

with $T_{ref} = 353$ K and $E = 2640\exp(-0.6\lambda) + 1183$, and then: $R_m = \int_0^{l_m} dz/\sigma(z)$.

The relationship between the activation overvoltage η_{act} and the current density is described by the Tafel equation. Unless otherwise stated, the values are those of Larminie and Dicks [27]:

$$\eta_{act} = a \ln(i/i_0) \quad \text{with}$$
$$a = 0.06 \text{ Volt} \quad \text{and} \quad i_0 = 0.67 \text{ A/m}^2 \quad (30)$$

The thermodynamic potential E_{Gibbs} is a function of the activities a_i of products and reagents at the electrodes:

$$E_{Gibbs} = -\frac{\Delta G^0(T)}{2F} - \eta_{conc} \quad \text{with}$$
$$\eta_{conc} = -\frac{RT}{2F} \ln\left(\frac{a_{H_2} a_{O_2}^{1/2}}{a_{H_2O}}\right) \quad (31)$$

$\Delta G^0(T)$ denotes the Gibbs energy of the reaction of hydrogen oxidation with all species activities equal to one. η_{conc} accounts for the concentration polarization, defined by reference to the standard potential E_0. Since the activities of gases are functions of their partial pressure p_i, η_{conc} is null only in some very particular cases when the partial pressure of oxygen, hydrogen and water vapor are simultaneously equal to 10^5 Pa. η_{conc} can be negative when the partial pressure of vapor is low. The activity of oxygen diffusing through liquid water is given by $K_{O_2} c_{O_2,l}/P_0$, where K_{O_2} is the Henry's coefficient, $c_{O_2,l}$ is the molar concentration of gas in water, and P_0 is the standard pressure [27]. It is then possible to derive the expression of the overpotential induced by oxygen diffusion in liquid water (32):

$$\Delta V = -\frac{RT}{4F} \ln\left(\frac{c_{O_2,l}(\text{cathode})}{c_{O_2,l}(\text{liquid–gas interface})}\right) = -\frac{RT}{4F} \ln\left(1 - \frac{i e_l}{4F D_{O_2-H_2O}} \frac{K_{O_2}}{p^l_{O_2}}\right) \quad (32)$$

Eq. (32) allows to estimate the order of magnitude of the maximal thickness of liquid overlaying the cathode: the simplest assumption consists in noticing that the potential drop ΔV cannot be superior to the fuel cell potential without liquid water $E(i)$ (33):

$$e_{max} = \frac{4F p_{O_2}}{i D_{O_2-H_2O} K_{O_2}} (1 - e^{-4FE(i)/RT}) \quad (33)$$

where $E(i)$ is given by (28).

Fig. 4 shows the evolution of liquid maximal thickness e_{max} as a function of the current density, using the parameters given by Bernardi and Verbrugge [22] and by Jaouen et al. [25] (Table 1). It appears immediately that the liquid maximal thickness is several orders of magnitude lower than the value required for evacuating water by gas diffusion (Fig. 3). As a consequence, the polarization curve resulting from this 1D model of MEA has the peculiar shape depicted in Fig. 5: the limiting current density i_l for which fuel cell potential becomes null is very close to

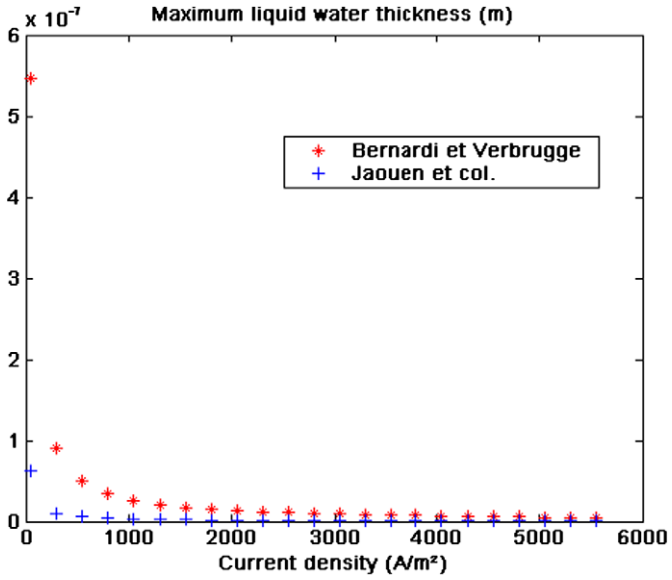

Fig. 4. Estimation of the thickness of liquid water e_{max}, necessary to reduce the cell voltage down to zero, according to Eq. (33). Parameters are those described in Section 2.2. Thickness of the porous backing layer: 450 μm; thickness of the membrane: 30 μm.

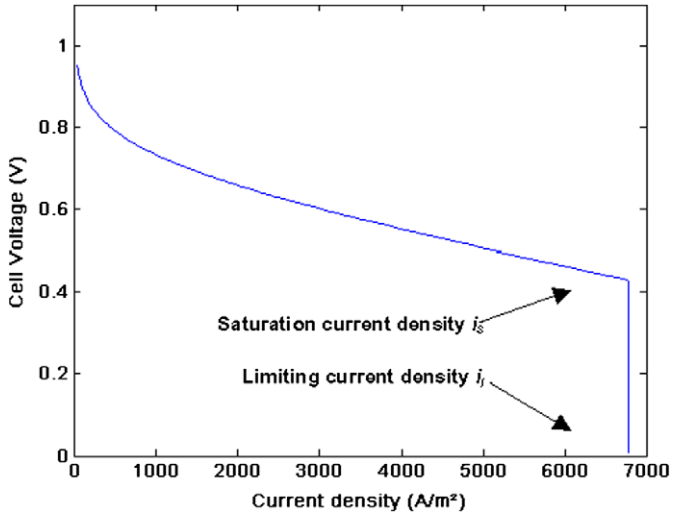

Fig. 5. Polarization curve of a PEMFC elementary cell described by the 1D model; a sharp fall in voltage occurs when the saturation vapor pressure is reached at the cathode; the limiting current density i_l is slightly higher than the saturation current density i_s but in practice, this difference is neglected. (Porous backing layers thickness: 450 μm; membrane thickness: 30 μm; air dew temperature: 79 °C (96% RH); dew temperature of hydrogen: 79 °C (96% RH); fuel cell temperature: 80 °C.)

the saturation current density i_s for which liquid water appears at the cathode: in practice, the difference between these two current densities is neglected and consequently, the 1D model do not allow the fuel cell current density to be greater than the value corresponding to vapor saturation at the cathode (i_s).

The shape of the polarization curve of flooded MEAs presented in Fig. 5 may not be realistic. However, it should be kept in mind that it results from simple approximations and that it characterizes the operation of a slice of the MEA that is (ideally) of infinitely small area. This polarization curve does not imply that the current density is null in the presence of liquid water but it defines, without any supplementary parameter and as a function of only the composition of the gases at the inlet of the slice, the value of the (local) limiting current density. It is shown in Section 3 that this polarization curve is interesting as a building block for a pseudo-2D model.

2.4. Comments about the 1D hypotheses

Several comments can be made about earlier assumptions:

- **Electrodes have a finite thickness and the liquid film grows in a porous medium.** Consequently, the liquid probably spreads over the solid phase without restricting so much the access of oxygen to the catalyst particles. However, it is difficult to estimate the real thickness of the liquid film in porous media. A simple assumption would consist in using a "shape factor" characterizing the ratio between the wet depth of the porous backing layer (estimated according to the mechanisms depicted in Section 2.3 and Fig. 3) and the real liquid film thickness on porous media: this parameter should be of the order of 10^3–10^4 to significantly modify the discrepancy between saturation current density i_s and limiting current density i_l. By comparison, the roughness factor giving the ratio between an electrode effective active surface and its plane area is usually of the order of 10^2.
- **The effects of the surface tension are ignored:** micro pores with different diameters and different hydrophilic and hydrophobic properties coexist in the electrodes and in the GDLs. In practice, only the pores with diameter greater than the capillary condensation threshold diameter will be saturated with water, whereas the other pores will remain free of liquid and permit the flow of gases in a partially saturated electrode or GDL [28]. In some 1D models, the presence of liquid water is accounted for through the introduction of a saturation ratio (the ratio of saturated volume to the total volume of the pore) [14,29–31]. The relation between the liquid water flux through the GDL and/or electrode and the saturation ratio can be described by means of Darcy's law using the relative permeability of individual phases [31].
- **The cell is not isothermal:** heat production by the MEA implies the existence of temperature gradient along the x-direction so that the first place where relative humidity reaches 100% may not be the cathode (where water is produced) but the air channel (where the temperature is the lowest). This issue must be addressed by coupling heat and mass transfer models and by addressing the effects of thermal diffusion [8].

3. Pseudo-2D approach

Molar changes along the gas channels are calculated by mass balance (Fig. 6):

$$\Delta \dot{m}_k = \pm \frac{N_k M_k \Delta S}{1000} \tag{34}$$

Where ΔS is the surface of a slice. The sign of the right-hand side of Eq. (34) depends on the direction of the flux of each species through the backing layer and on the direction of gas flows in the channels. The model can be applied to cocurrent gas flows (hydrogen and air flow in the same direction) and to countercurrent flows. All the results given in the followings apply to cocurrent flows. Mass fluxes through the MEA are determined starting from the cell potential and gas composition at the inlet of each slice. Gas flow rates at the inlet of the fuel cell are defined by a stoichiometric coefficient, which corresponds to the ratio between the effective mass flow rate and the amount consumed by the fuel cell (35). Gas consumption and current densities are linked by Eq. (36). It is possible to simulate a dead-end hydrogen channel, that is to say with a null hydrogen outlet flow.

$$St_{\mathrm{H_2}} = \frac{\dot{m}_{\mathrm{H_2,inlet}} - \dot{m}_{\mathrm{H_2,outlet}}}{\dot{m}_{\mathrm{H_2,inlet}}} \quad \text{and}$$
$$St_{\mathrm{O_2}} = \frac{\dot{m}_{\mathrm{O_2,inlet}} - \dot{m}_{\mathrm{O_2,outlet}}}{\dot{m}_{\mathrm{O_2,inlet}}} \tag{35}$$
$$\dot{m}_{\mathrm{H_2,inlet}} - \dot{m}_{\mathrm{H_2,outlet}} = \frac{\sum_{\mathrm{slices}} i_{\mathrm{slice}} \Delta S}{1000 M_{\mathrm{H_2}} F} \quad \text{and}$$

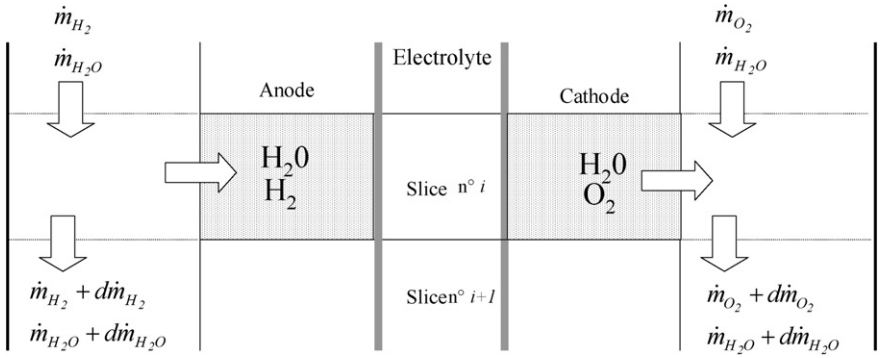

Fig. 6. Gas flow rate variation in the feeding channels.

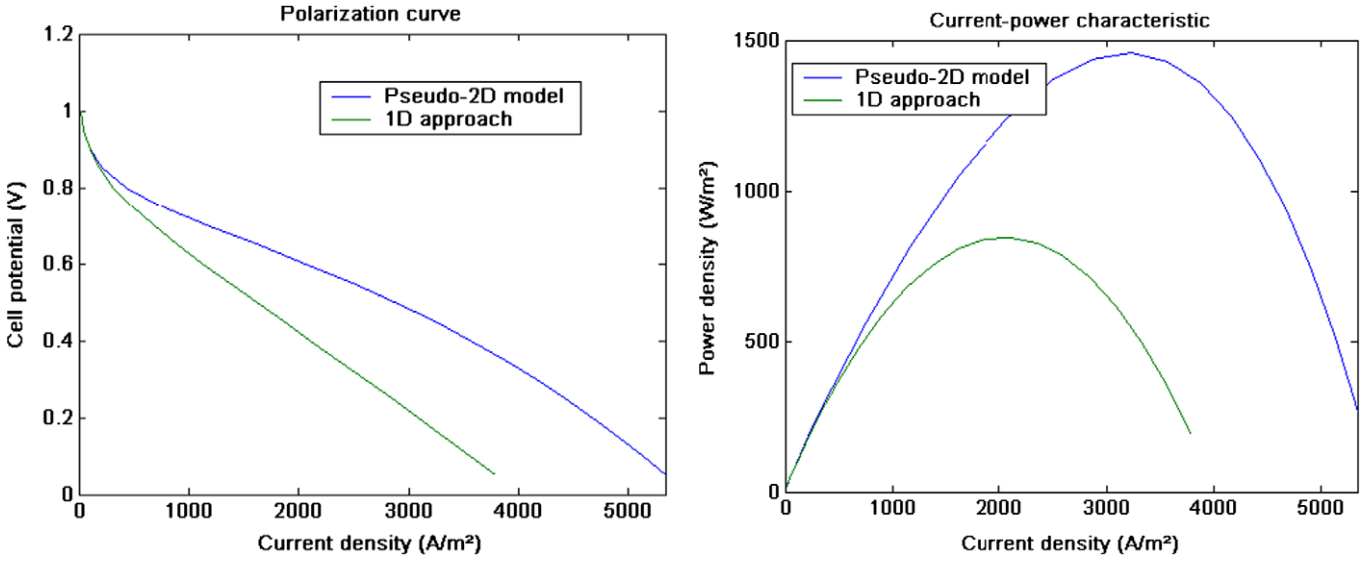

(a) (b)

Fig. 7. Polarization curves and current-power characteristic of a PEMFC cell, according to the 1D and pseudo-2D models. (Backing layers thickness: 230 μm; membrane thickness: 125 μm; inlet air RH: 90%; hydrogen inlet RH: 5%; temperature: 80 °C; $St_{H_2} = 1.0$; $St_{O_2} = 8.0$.) The results of the pseudo-2D model converge toward those of the 1D approach when St_{H_2} and St_{O_2} are infinite.

$$\dot{m}_{O_2,\text{inlet}} - \dot{m}_{O_2,\text{outlet}} = \frac{\sum_{\text{slices}} i_{\text{slice}} \Delta S}{1000 M_{O_2} F} \tag{36}$$

The bipolar plates being equipotential, the principle of the algorithm consists in calculating for each slice the current density that matches the required desired voltage. If vapor saturation pressure is reached at the cathode, the current density is set equal to the saturation current density i_s (Fig. 5), which value varies locally as a function of gas characteristics at slice inlet.

Note that the pseudo-2D and 1D approach converge when St_{H_2} and St_{O_2} are infinite, since there is no change in the gas composition in the channels.

4. Results

4.1. Results without water flooding

Fig. 7(a) and (b) shows the discrepancies that exist between the polarization curves yielded by a 1D approach and by the pseudo-2D models, when the hydrogen excess is low ($St_{H_2} = 1.0$, which correspond to a dead-end mode with regular purges) and with a strong excess of air at cathode side ($St_{O_2} = 8.0$) in order to avoid water condensation. However, air is strongly humidified (90% RH) whereas hydrogen can be considered as dry (5% RH). These operating conditions maximize the discrepancy between the two models that is of about 70% for the optimum of power (with regard to the value of the 1D model). The better performances obtained with the pseudo-2D model are explained by water transfer trough the membrane from cathode to anode (Fig. 8(a)), which progressively balances water activities at both sides, improves hydration and reduces ohmic resistance (Fig. 8(b)). Further along the channels, a reverse water flux is observed: it is a result of hydrogen consumption, which entails a rise in vapor partial pressure (considering that the total pressure remains constant). This reverse flux occurs more downstream at strong current densities due to mass transfer resistance in the membrane, which limits the amount of water passing from one side to the other. On top of that, electroosmosis reduces the water flux through the membrane at high current density, as it can be observed in Fig. 8(a), on the first slices.

Fig. 8(c) shows that the current density produced by the fuel cell is non-homogeneous: it increases continuously and signifi-

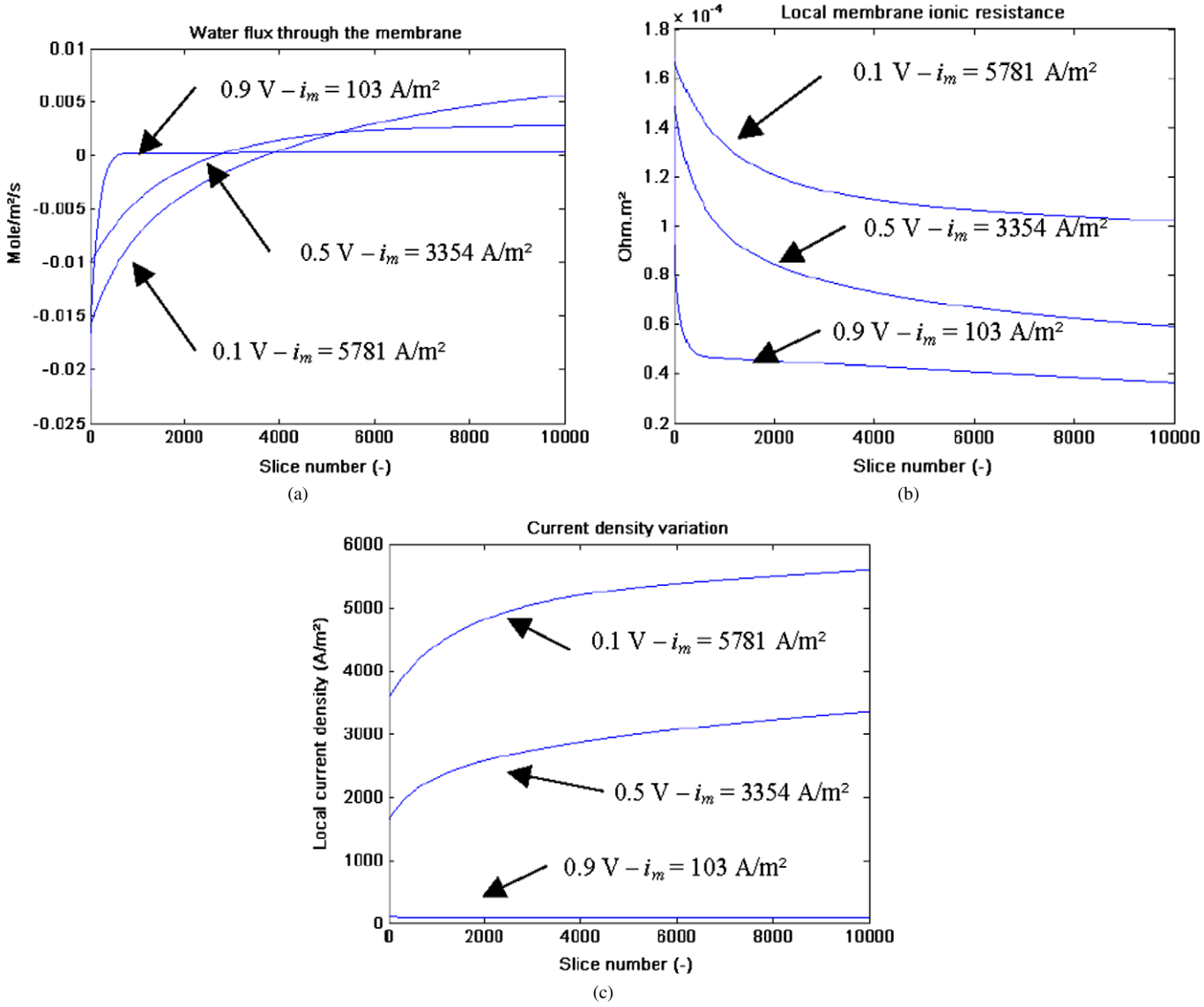

Fig. 8. Spatial distribution of water flux through the membrane (a), ohmic resistance (b), and local current density (c) along the feeding channels for three values of the cell voltage E. (Backing layers thickness: 230 μm; membrane thickness: 125 μm; inlet air RH: 90%; hydrogen inlet RH: 5%; temperature: 80 °C; $St_{H_2} = 1.0$; $St_{O2} = 8.0$.)

cantly between gas inlet and outlet. This is the result of changes in gas composition, modifying both the ohmic drop (26) and the concentration polarization (28).

Eq. (35) yields the local heat flux density as a function of current density (Fig. 8(c)) and fuel cell potential E, with $\Delta H_{H_2+1/2O_2\to H_2O_v}(T)$ the hydrogen Lower Heating Value. Fig. 9(a) depicts the variations of the heat flux density between the gas inlet and outlet at different cell potentials. In Fig. 9(b), this results is expressed in terms of relative span (or degree of relative heterogeneity), by reference to the mean value: the maximum of heat flux heterogeneity is always observed in the vicinity of the optimum of electric power of the fuel cell.

$$\dot{q} = i\left(-\frac{\Delta H_{H_2+1/2O_2\to H_2O_v}(T)}{2F} - E\right) \tag{37}$$

4.2. Comparison of 1D and pseudo-2D results in the presence of water flooding

With 1D approaches (Fig. 5), the inlet gases should be very wet and the current density very high to reach saturation [15]. On the other hand, the pseudo-2D model takes account of the increase in vapor partial pressure along the channels and liquid water appears more easily in the cell (Fig. 10 (a) and (b)), but mostly in the slices that are close to the exit (Fig. 11 (a) and (b)): by comparison with the last section, a simple decrease in the air sweeping ($St_{O_2} = 3.0$) induces water condensation. The presence of water entails a strong inflexion of the polarization curve at high current density and a drop of the limiting current density (Fig. 10(a)). It is interesting to note that although the power optima observed in Fig. 10(b) are similar, the value of the pseudo-2D model corresponds to a much lower current density, which means that the fuel cell electrical effi-

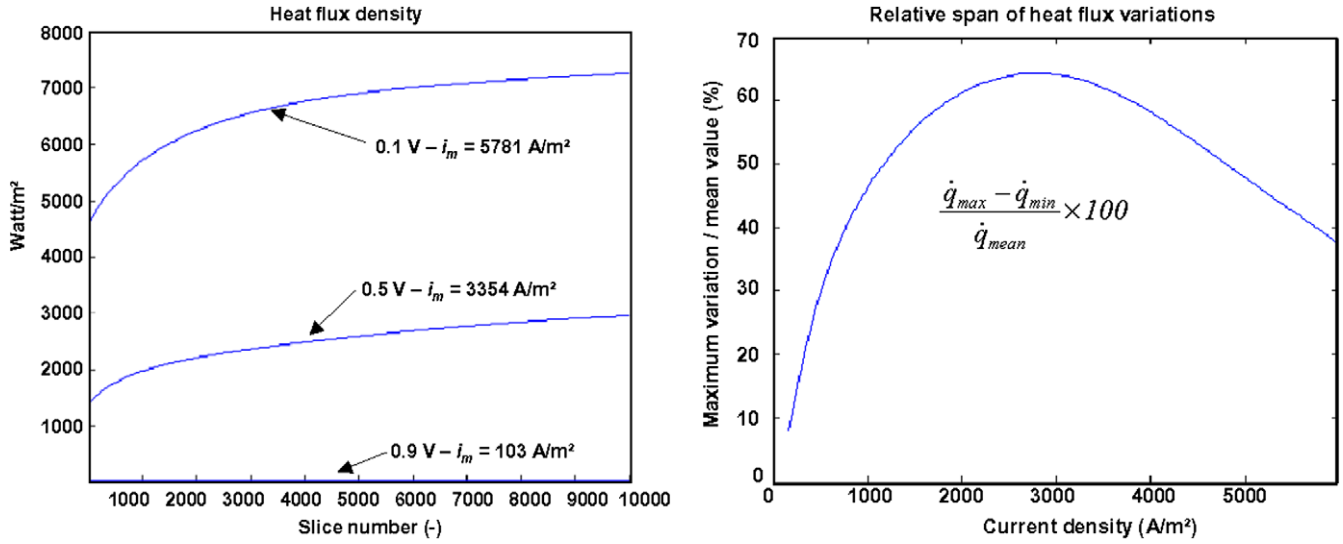

(a) (b)

Fig. 9. (a) Spatial distribution of the heat flux produced by the EME for 3 values of cell voltage. (b) Relative span of heat flux variations. (Backing layers thickness: 230 μm; membrane thickness: 125 μm; inlet air RH: 90%; hydrogen inlet RH: 5%; temperature: 80 °C; $St_{H_2} = 1.0$; $St_{O_2} = 8.0$.)

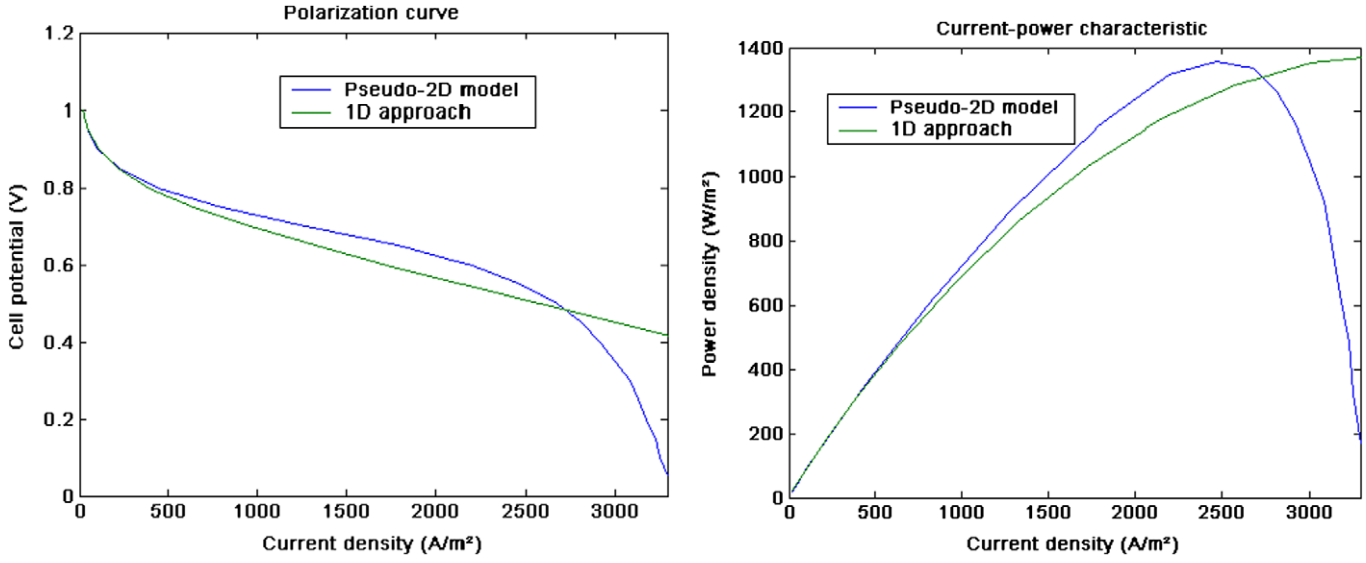

(a) (b)

Fig. 10. Polarization curves and current-power characteristics of a PEMFC cell, according to the 1D and pseudo-2D models; water flooding is only observed with the pseudo-2D model. (Backing layers thickness: 230 μm; membrane thickness: 125 μm; inlet air RH: 90%; hydrogen inlet RH: 20%; temperature: 80 °C; $St_{H_2} = 2.0$; $St_{O_2} = 3.0$.) The results of the pseudo-2D model converge toward those of the 1D approach when St_{H_2} and St_{O_2} are infinite.

ciency is better. Once again, the good performances obtained with the pseudo-2D model are explained by the enhancement of membrane hydration due to the water flux from cathode to anode.

The condensation of water implies a drastic fall of local current density (Fig. 11(a)): downstream the location where liquid appears, the current density equals the saturation current density i_s, which decreases with hydrogen and oxygen consumption along the channels. The ionic resistance of the membrane decreases simultaneously (Fig. 11(b)) because of its better hydration. However, one can notice that this fall of the membrane resistance along the feeding channels has nothing to do with the Schroeder's paradox sometimes observed with flooded EME; on the contrary, a continuous increase of the overall resistance is observed (Fig. 12).

On account of the various effects described above, the heat flux produced by a flooded cell is highly heterogeneous (Fig. 13 (a) and (b)): the spatial heterogeneity reaches its maximum in the vicinity of the limiting current i_l (Fig. 13(b)); the discontinuity of the slope observed near $i = 1800$ A/m^2 corresponds to water condensation in the cell.

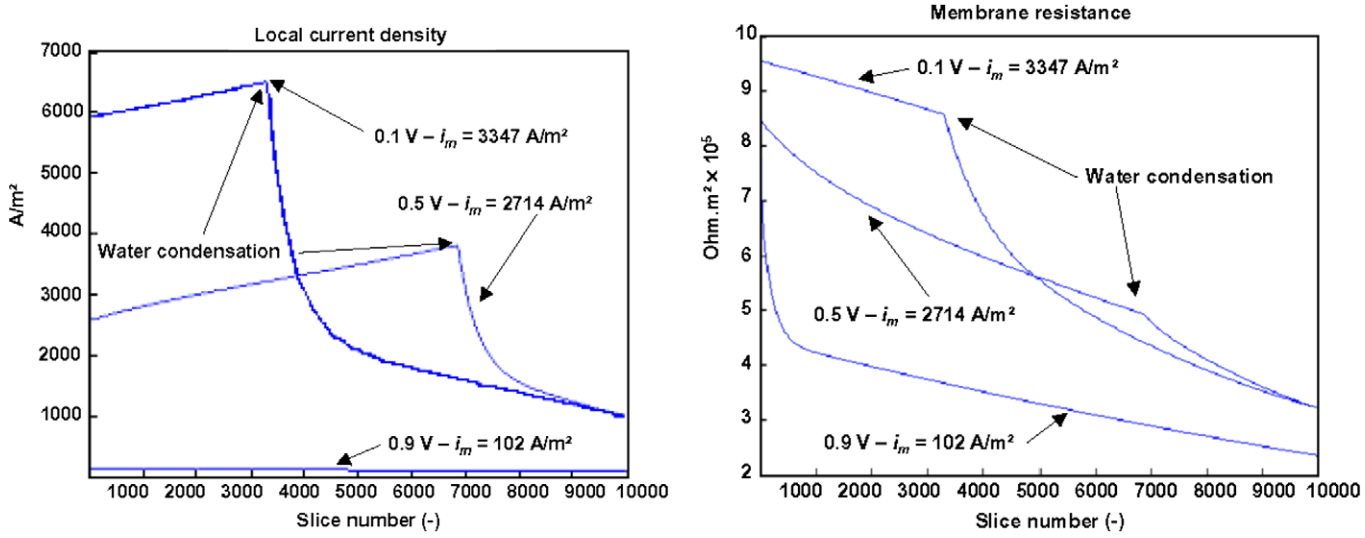

(a) (b)

Fig. 11. Distribution of the membrane ohmic resistance and of local current density along the gas channels for three values of the cell voltage E. (Backing layers thickness: 230 μm; membrane thickness: 125 μm; inlet air RH: 90%; hydrogen inlet RH: 20%; temperature: 80 °C; $St_{H_2} = 2.0$; $St_{O2} = 3.0$.)

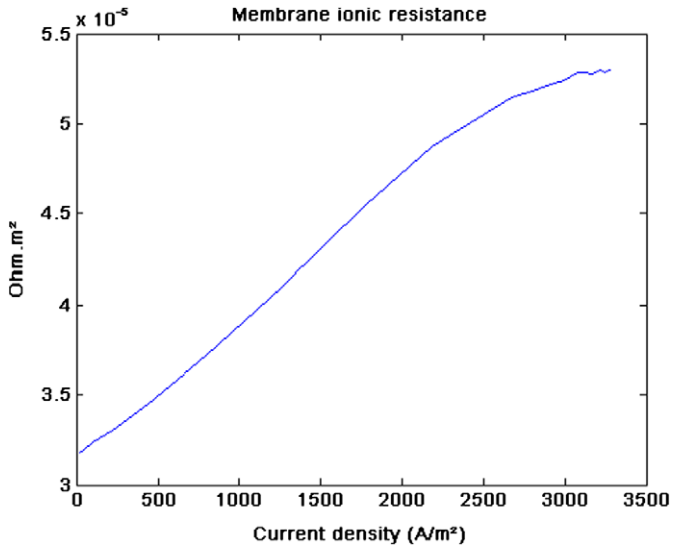

Fig. 12. Membrane overall ionic (ohmic) resistance as a function of the current density in a flooded cell. (Backing layers thickness: 230 μm; membrane thickness: 125 μm; inlet air RH: 90%; hydrogen inlet RH: 20%; temperature: 80 °C; $St_{H_2} = 2.0$; $St_{O_2} = 3.0$.)

5. Discussion

As underlined in the previous section, the pseudo-2D model puts forward the presence of strong heterogeneities in local current density, in water flux through the membrane, in membrane ionic resistance and in heat flux density (Figs. 8–9, 11 and 13). These heterogeneities are observed even in the absence of condensation but they are stronger in the presence of liquid water on the electrodes: in this case, the span (maximum value minus minimum value) can reach up to 100% of the mean value for the current density and more than 150% for the heat flux density (Fig. 13(b)). Following this work, an experimental study consisting in the implementation of a multi-instrumented single Polymer Exchange Membrane Fuel Cell (PEMFC) was carried out. This fuel cell has parallel gas channels (i.e. a 2D geometry) and the MEA is divided into twenty 1.4 cm successive segments electrically connected only after the measurement of local current. The temperature of each segment was also measured. Since the fuel cell is built from transparent PMMA (PolyMethyl MethAcrylate), an additional observable is the location where liquid water appears in the channels (Maranzana et al. [29,33]). Strong heterogeneities in current density were observed, confirming the theoretical results. These heterogeneities are highly dependent on the operating conditions: in the absence of liquid water in the channel (and in co-flow configuration), the local current density is the lowest near the gas inlets (where the membrane is the driest) whereas it is the highest near the gas outlets (where gases and the membrane are humidified by the water produced by the fuel cell). This observation confirms the tendency observed in Fig. 8(c). On the other hand, in the presence of condensation, the optimum in current density is correlated to the appearance of liquid water in the channel, which confirms the results depicted in Fig. 11(a). Note that at this stage, and considering both the simplifying hypotheses of the model and the limitations of the experimental set up, the parallel between theoretical results and local measurements is only qualitative. In terms of thermal dissipation, it appears that the temperature profile is strongly correlated with the current density distribution whereas the results of the pseudo-2D model suggest a correlation between the current density and the heat flux density (Figs. 8(c) and 9(a) or Figs. 11(a) and 13(a)).

Also rare, several studies were presented in the literature about the measurement of current density distribution in the plane of a cell [32–38], with various techniques. Although discussing these techniques would be out of the scope of this paper, it should be noted that they are generally applied to fuel cells with serpentine channels, which makes the comparison with simple models (assuming parallel channels) difficult. However,

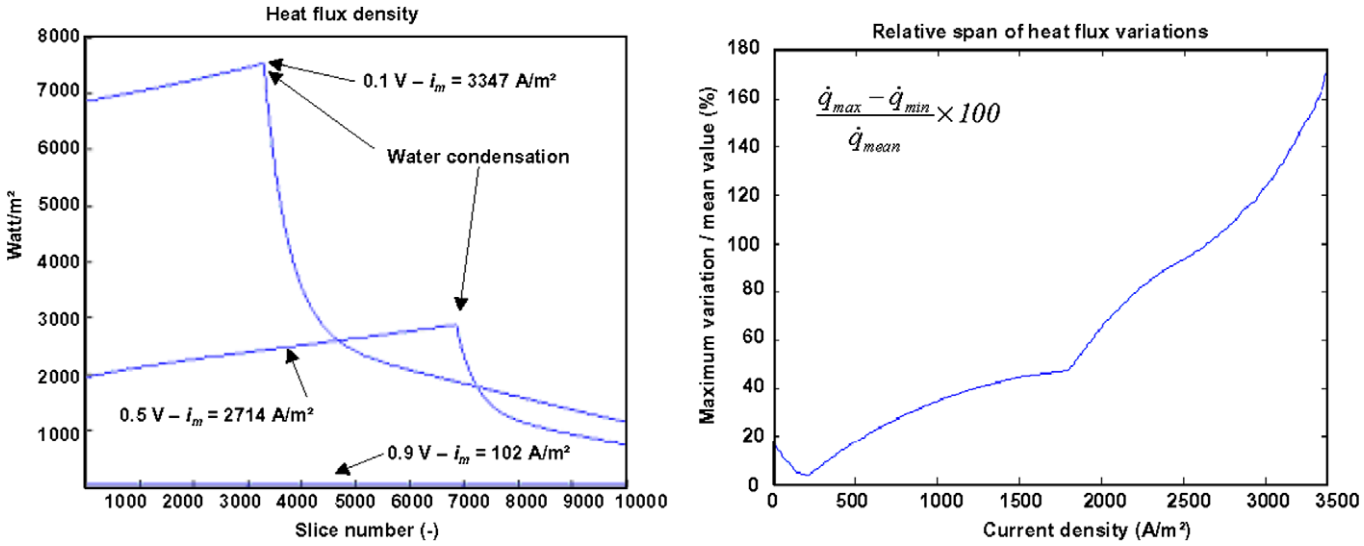

(a) (b)

Fig. 13. (a) Spatial distribution of the heat flux produced by the EME for 3 values of cell voltage in a flooded cell. (b) Relative span of heat flux variations as a function of the current density. (Backing layers thickness: 230 μm; membrane thickness: 125 μm; inlet air RH: 90%; hydrogen inlet RH: 20%; temperature: 80 °C; $St_{H_2} = 2.0$; $St_{O_2} = 3.0$.)

Cleghorn et al. [33] and Brett et al. [34] agreed about the existence of mechanisms of internal humidification (i.e. improvement of fuel cell performances along the gas channels because of water production).

In most of the cases, the shape of the current density profiles is strongly linked to the fuel cell operating condition in terms of gas humidification and stoichiometry.

6. Conclusions

The main contributions of the pseudo-2D approach are probably to underline the limits of the mono-dimensional modelling of the MEA and to put forward the presence—in certain conditions—of strong local heterogeneities in fuel cell operation, now validated by some experimental works. Some uncertainties and assumptions subsist that are not fully satisfying on a physical point of view (Section 2.4) but on the other hand, the model allows to determine the fuel cell limiting current density as a function of the gas composition and stoichiometry only. Note also that these difficulties do not seem to be linked to the geometrical simplification of the model and do not justify the use of fully multidimensional models, at least for qualitative investigations. However, this approach could be extended to the modelling of cross-flow and counter-flow configurations. Finally, the place of water condensation depending on local temperature, the coupling of this model with a multidimensional heat transfer model could be one of the next steps of this work.

References

[1] V. Gurau, H. Liu, S. Kadac, Two-dimensional model for proton exchange membrane fuel cells, AIChE Journal 44 (11) (1998) 2410–2422.

[2] I.M. Hsing, P. Futerko, Two-dimensional simulation of water transport in polymer electrolyte fuel cells, Chemical Engineering Science 55 (19) (2000) 4209–4218.

[3] S. Dutta, S. Shimpalee, J.W. Van Zee, Numerical prediction of mass-exchange between cathode and anode channels in a PEM fuel cell, International Journal of Heat and Mass Transfer 44 (11) (2001) 2029–2042.

[4] A.A. Kulikovsky, Quasi-3D modelling of water transport in polymer electrolyte fuel cells, Journal of the Electrochemical Society 150 (11) (2003) A1432–A1439.

[5] N.P. Siegel, N.W. Ellis, D.J. Nelson, M.R. Van Sparkovsky, A two-dimensional computational model with liquid water transport, Journal of Power Sources 128 (2) (2004) 173–184.

[6] P. Costamagna, Transport phenomena in polymeric membrane fuel cells, Chemical Engineering Science 56 (2) (2001) 323–332.

[7] P. Costamagna, S. Srinivasan, Quantum jumps in the PEMFC science and technology from the 1960s to the year 2000: Part II. Engineering, technology development and application aspects, Journal of Power Sources 102 (1–2) (2001) 253–269.

[8] N. Djilali, D. Lu, Influence of heat transfer on gas and water transport in fuel cells, International Journal of Thermal Sciences 41 (1) (2002) 29–40.

[9] K. Dannenberg, P. Ekdunge, G. Lindbergh, Mathematical model of the PEMFC, Journal of Applied Electrochemistry 30 (12) (2000) 1377–1387.

[10] G.J.M. Janssen, A phenomenological model of water transport in a proton exchange membrane fuel cell, Journal of the Electrochemical Society 148 (12) (2001) A1313–A1323.

[11] P. Berg, K. Promislow, J.St. Pierre, J. Strümper, B. Wetton, Water management in PEM fuel cells, Journal of the Electrochemical Society 151 (3) (2004) A341–A353.

[12] M. Bautista, Y. Bultel, P. Ozil, Polymer electrolyte membrane Fuel Cell modelling: dc and ac solutions, Chemical Engineering Research and Design, Part A 82 (a7) (2004) 907–917.

[13] S.A. Freundberger, M. Santis, I.A. Schneider, A. Wokaun, F.N. Büchi, In-plane effects in large-scale PEMFCs, Journal of the Electrochemical Society 153 (2) (2006) A396–A405.

[14] D.A. McKay, W.T. Ott, A.G. Stefanopoulou, Modeling, Parameter identification, and validation of reactant and water dynamics for a fuel cell stack, in: Proceedings of IMECE'05, 2005 ASME International Mechanical Engineering Congress and Exposition, November 5–11, 2005, Orlando, FL, USA.

[15] J. Ramousse, J. Deseure, S. Didierjean, O. Lottin, D. Maillet, Modelling of heat, mass and charge transfers in a PEMFC, Journal of Power Sources 145 (2) (2005) 416–427.
[16] J. Ramousse, J. Deseure, S. Didierjean, O. Lottin, D, Maillet, Modelling of heat, mass and charge transfers in a PEMFC single cell, in: Fuel Cells Sciences and Technology, Scientific Advances in Fuel Cell Systems, München, Germany, 6–7 October 2004.
[17] T. Okada, G. Xie, Y. Tanabe, Theory of water management at the anode side of polymer electrolyte fuel cell membranes, Journal of Electroanalytical Chemistry 413 (1–2) (1996) 49–65.
[18] T. Okada, G. Xie, M. Meeg, Simulation for water management in membranes for polymer electrolyte fuel cells, Electrochimica Acta 43 (14-15) (1998) 2141–2155.
[19] T.E. Springer, T.A. Zawodzinski, S. Gottesfeld, Polymer electrolyte fuel cell model, Journal of the Electrochemical Society 138 (8) (1991) 2334–2342.
[20] T.E. Springer, T.A. Zawodzinski, M.S. Wilson, S. Gottesfeld, Characterization of polymer electrolyte fuel cells using AC impedance spectroscopy, Journal of the Electrochemical Society 143 (2) (1996) 587–599.
[21] D. Arnost, P. Schneider, Dynamic transport of multicomponent mixtures of gases in porous solids, The Chemical Engineering Journal and the Biochemical Engineering Journal 57 (2) (1995) 91–99.
[22] D.M. Bernardi, M.W. Verbrugge, Mathematical model of a gas diffusion electrode bonded to a polymer electrolyte, AIChE Journal 37 (8) (1991) 1151–1163.
[23] J.T. Hinatsu, M. Mizuhata, H. Takenaka, Water uptake of perfluorosulfonic acid membranes from liquid water and water vapor, Journal of the Electrochemical Society 141 (6) (1994) 1493–1498.
[24] R.B. Bird, W.E. Stewart, E.N. Lightfoot, Transport Phenomena, John Wiley & Sons, New York, 1960.
[25] F. Jaouen, G. Lindbergh, G. Sundholm, Investigation of mass-transport limitations in the solid polymer fuel cell cathode, Journal of the Electrochemical Society 149 (2002) A437–A447.
[26] W. Neubrand, Modelbilung und Simulation von Elektromembranverfahren thesis, Logos, 1999.
[27] Larminie, Dicks, Fuel Cell Systems Explained, Wiley, 2003.
[28] Z. Liu, Z. Mao, C. Wang, A two dimensional partial flooding model for PEMFC, Journal of Power Sources 158 (2) (2006) 1229–1239.
[29] G. Maranzana, S. Chupin, T. Colinart, O. Lottin, S. Didierjean, Pseudo-2D polarization model of Polymer Exchange Membrane Fuel Cell including mass transport limitation due to flooding. Numerical simulation and comparison with experimental results, in: Proc. Hydrogen and Fuel Cell 2007, International Conference and Trade Show, pp. 460–469, Vancouver Convention & Exhibition Centre, Vancouver BC, Canada, April 29–May 2, 2007.
[30] J.H. Nam, M. Kaviany, Effective diffusivity and water-saturation distribution in single- and two-layer PEMFC diffusion medium, International Journal of Heat and Mass Transfer 46 (24) (2003) 4595–4611.
[31] T. Colinart, O. Lottin, B. Antoine, S. Didierjean, G. Maranzana, C. Moyne, Pseudo 2D polarization model of a Polymer Exchange Membrane Fuel Cell including liquid water transport, in: 5th European Thermal-Sciences Conference, 18–22 May 2008, Eindhoven, the Netherlands.
[32] G. Maranzana, O. Lottin, S. Chupin, T. Colinart, S. Didierjean, A multi-instrumented polymer exchange membrane fuel cell, Observation of the in-plane non-homogeneities, Journal of Power Sources, in press, doi: 10.1016/j.jpowsour.2008.03.002.
[33] S.J.C. Cleghorn, C.R. Derouin, M.S. Wilson, S. Gottesfeld, A printed circuit board approach to measuring current distribution in a fuel cell, Journal of Applied Electrochemistry 28 (7) (1998) 663–672.
[34] D.J.L. Brett, S. Atkins, N.P. Brandon, N. Vasileiadis, V. Vesovic, A.R. Kucernak, Membrane resistance and current distribution measurements under various operating conditions in a polymer electrolyte fuel cell, Journal of Power Sources 172 (2007) 2–13.
[35] J. Stumper, S.A. Campbell, D.P. Wilkinson, M.C. Johnson, M. Davis, In-situ methods for the determination of current distributions in PEM fuel cells, Electrochemica Acta 43 (24) (1998) 3773–3783.
[36] M.M. Mench, C.Y. Wang, M. Ishikawa, In Situ current distribution measurements in polymer electrolyte fuel cells, Journal of the Electrochemical Society 150 (8) (2003) A1052–A1059.
[37] Z. Liu, Z. Mao, B. Wu, L. Wang, V.M. Schmidt, Current density distribution in PEFC, Journal of Power Sources 141 (2) (2005) 205–210.
[38] H. Sun, G. Zhang, L. Guo, H. Liu, A novel technique for measuring current distributions in PEM fuel cells, Journal of Power Sources 158 (1) (2006) 326–332.